PREPRINT, SUBMITTED TO PHYSICS OF PLASMAS. DO NOT DISTRIBUTE.

Parallel Velocity Diffusion and Slowing-Down Rate from Long-Range Collisions in a Magnetized Plasma

Daniel H.E. Dubin[1]

Department of Physics, University of California at San Diego, La Jolla, California 92093

(Dated: 18 March 2014)

This paper derives an expression for the rate of collisional slowing of charges in a magnetized plasma for which $r_c < \lambda_D$, where r_c is the mean thermal cyclotron radius and λ_D is the Debye length. The rate depends on a new fundamental length scale d that separates collisions into two impact parameter ranges that yield different slowing rates: a Boltzmann rate due to isolated binary collisions for impact parameters $\rho < d$; and a Fokker-Planck rate due to multiple small scatterings for $\rho > d$. Slowing due to Boltzmann collisions is also shown to depend on the sign of the Coulomb interaction: for repulsive interactions the slowing is enhanced by "collisional caging," while for attractive interactions the Boltzmann slowing rate is zero.

I. INTRODUCTION

The rate at which charged particles slow due to collisions with surrounding charges is important to a number of physical processes, including runaway electrons in magnetically-confined fusion plasmas,[1] magnetic reconnection in collisional regimes,[2] and the growth rate of nonideal plasma instabilities such as collisional drift waves.[3] In many such cases, a magnetic field affects the plasma dynamics. This paper presents a calculation of the slowing-down rate in a weakly-coupled thermal plasma for which $r_c < \lambda_D$ where r_c is the mean thermal cyclotron radius of the two colliding species and λ_D is the Debye length. We focus on collisional slowing of motion parallel to the magnetic field, due only to charge-charge collisions, with the charges treated as classical point particles. For electrons with density n_e in a magnetic field B, the regime $r_{\rm ce} < \lambda_{\rm De}$ requires $B > 32$ gauss $\sqrt{n_e/10^8{\rm cm}^{-3}}$. Many plasmas have one or more species which satisfy $r_c < \lambda_D$, such as the low density edge in a tokamak plasma, the solar plasma near sunspots, and non-neutral plasmas. However, a precise theory of the parallel slowing rate has not been formulated for plasmas in this regime.

We will show that parallel slowing in this regime can be strongly enhanced by collisions with impact parameters ρ in the range $r_c < \rho < \lambda_D$. Such collisions are described by guiding centers interacting as they move in one dimension (1D) along the magnetic field (see Fig. 1).[4] These 1D long-range (compared to r_c) collisions are not included in the well-known classical collision rates[5,6] or transport coefficients[7–9] produced by short-range ($\rho < r_c$) collisions that scatter the cyclotron velocity vector. Long-range collisions have been shown previously to lead to enhanced cross-field diffusion,[10,11] viscosity,[12] and thermal conduction[13,14] in the regime $r_c < \lambda_D$.

We will also show that these 1D long-range collisions separate into two types: Boltzmann collisions where the colliding particles can be treated as isolated pairs, and Fokker-Planck (FP) collisions where many weak collisions are happening simultaneously. We will find that the Boltzmann collisions occur for impact parameters in the range $\rho < d$, whereas the FP collisions occur for $\rho > d$. Here, we introduce the distance d, a novel but fundamental length scale given by the expression

$$d \equiv \left[(|e_i e_j|/\mu)^3/D^2\right]^{1/5}. \tag{1}$$

Here e_i and e_j are the charges of the colliding species i and j, $\mu \equiv m_i m_j(m_i + m_j)$ is their

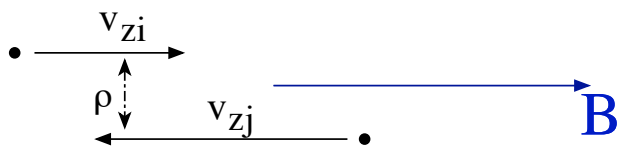

FIG. 1. 1D collision between two guiding centers labelled i and j on field lines separated by impact parameter ρ, where $\rho > r_c$.

reduced mass, and $D = D_i + D_j$ is the diffusion coefficient for relative parallel velocity, with D_i and D_j the parallel velocity diffusion coefficients[6] for each species. The parallel slowing down rate ν_i of species i is related to the diffusion coefficient D_i by the Einstein relation

$$\nu_i = D_i m_i / T \tag{2}$$

where T is the plasma temperature.

In order to see how d enters the theory of 1D long-range collisions, note that Boltzmann theory for such collisions assumes an isolated 1D binary interaction. Such an interaction is shown in Fig. 1. Two guiding centers on different field lines separated by distance $\rho > r_c$ approach one another. Energy and momentum conservation then imply the two charges either reflect from one another, exchanging their parallel velocities, or pass by, with velocities unchanged. In Boltzmann theory, only those collisions that result in reflections have an effect on the slowing rate. Furthermore, reflections via the Coulomb potential occur only if the initial relative parallel speed $|\mathrm{v}_{z_i} - \mathrm{v}_{z_j}|$ is less than $(2e_i e_j/\mu\rho)^{1/2}$. This sets a timescale $t_B \equiv \rho(|e_i e_j|/\mu\rho)^{-1/2}$ for the reflections. This timescale becomes large for large ρ because well-separated particles must move slowly for their weak interaction to produce a reflection.

However, the collision can be regarded as isolated only if surrounding plasma charges do not interfere. These surrounding particles cause the colliding pair to diffuse in parallel velocity during the collision, and this diffusion must be small over the time t_B in order for the Boltzmann analysis to be valid. That is, $(Dt_B)^{1/2} < (|e_i e_j|/\mu\rho)^{1/2}$. Substituting for t_B and rearranging shows that only for $\rho < d$ is Boltzmann theory valid. On the other hand, for $\rho > d$, particles diffuse in velocity before a collision can be completed so reflections need not be considered. This is the regime where FP theory works.

We will therefore derive the slowing down rate for each theory, applying the results only to their relevant impact parameter range. We will then test this intuition using a Monte-Carlo

simulation based on a nonlinear Langevin equation that describes the Coulomb interaction between a particle pair, and also includes the diffusive influence of other particles on the pair.

In the Monte Carlo simulation, we will find that in the Boltzmann regime $\rho < d$, the collision rate is enhanced by the effect of "collisional caging,"[10] for like-sign particles (with $e_i e_j > 0$). That is, 1D collisions do not occur only once: parallel velocity diffusion due to the interactions of the colliding pair with surrounding charges eventually causes the relative velocity of the pair to reverse, so that the pair collides again. The correlation time of such a collision is enhanced by the effect of surrounding particles; hence the term collisional caging.

Caging is usually associated with strongly-coupled systems like liquids, but it occurs here, in a weakly-coupled plasma, because of the 1D dynamics imposed by the strong magnetic field. In contrast, multiple encounters happen rarely if the charges can wander in 2 or 3 dimensions. A similar caging effect was previously found to enhance both plasma viscosity[15] and spatial diffusion across the magnetic field.[4]

The distance d is not relevant for the 3D collisions considered in previous theories of collisional slowing. For 3D collisions, where the particle cyclotron velocity is scattered, Boltzmann theory and FP theory give the same answer for the collision rate, since it is dominated by small angle scattering.[6] But small angle scattering does not occur in 1D collisions, and consequently Boltzmann and FP theory give different results. For example, for isolated 1D collisions between oppositely-charged particles, there are no reflections and particles simply pass by without net velocity change. Hence, Boltzmann analysis would imply no collisional slowing from such collisions. However, we will see that FP analysis yields a finite result that is independent of the sign of the charges.

In Sec. II, we set up the collisional slowing problem using a Green-Kubo expression for parallel velocity diffusion. In Sec. III, we evaluate the Green-Kubo formula by using the simplest version of FP theory for 1D long-range collisions, which employs the technique of Integration Along Unperturbed Orbits (IUO). In Sec. IV, we derive the slowing rate using Boltzmann theory, showing that the result differs from the previous FP theory. In Sec. V, we introduce a Langevin model for the collisional dynamics and reconsider FP theory based on this model, without assuming IUO. We show that the answer for the slowing rate is the same as for the previous FP theory assuming IUO.

In Sec. VI, we simulate the Langevin model without making any approximations, using

a Monte Carlo method, and connect the results of the model to the theory. We find an enhancement of the diffusion coefficient (and hence the slowing rate) due to the aforementioned collisional caging effect, provided the colliding charges are of like sign. This enhancement depends on the velocity diffusion coefficient itself, and is largest as $D \to 0^+$. In Sec. VII, we consider this limit by rescaling variables in such a way that the Langevin equations of motion are independent of D in the $D \to 0^+$ limit. In Sec. VIII we consider an equivalent Fokker-Planck model of the $D \to 0^+$ limit, and rederive the diffusion coefficient as a test of the MC simulation. In Sec. IX we summarize the results and use them to evaluate the diffusion coefficient and slowing rate to logarithmic accuracy. In Sec. X we discuss the results. In the Appendix we include details of the numerical solution of the FP equation used in Sec. VIII.

II. GREEN-KUBO FORMULA FOR VELOCITY DIFFUSION

The equation of motion for the axial velocity of charge i in a plasma of N charges is

$$m_i \frac{d\mathrm{v}_{zi}}{dt} = \sum_{j\neq i}^{N} e_i e_j \frac{z_i - z_j}{|r_i - r_j|^3}\,. \tag{3}$$

By considering the velocity to be a stochastic process, the velocity diffusion coefficient D_i for particle i can be obtained from the Green-Kubo formula

$$D_i = \int_0^\infty dt \left\langle \frac{d\mathrm{v}_{zi}}{dt}(t) \frac{d\mathrm{v}_{zi}}{dt}(0) \right\rangle, \tag{4}$$

where the average is over an ensemble of realizations, i.e. over different initial positions and velocities of the plasma particles. We assume that the plasma is weakly-coupled, so only 2 particle collisions need be considered, and the only important terms in Eq. (3) involve particle pairs correlated only to their own initial positions:

$$D_i = \sum_{j\neq i}^{N} \left(\frac{e_i e_j}{m_i}\right)^2 \int_0^\infty dt \left\langle \frac{z_i(t) - z_j(t)}{|r_i(t) - r_j(t)|^3} \frac{z_i(0) - z_j(0)}{|r_i(0) - r_j(0)|^3} \right\rangle. \tag{5}$$

By directly evaluating the average as an integral over relative position and velocity of particles i and j, Eq. (5) can be written as

$$D_i = \sum_{j} \left(\frac{e_i e_j}{m_i}\right)^2 N_j \int_0^\infty dt \int \frac{d^3 r_0}{V} \int dv_{z_0} f_{ij}(v_{z_0}) \left\langle \frac{z(t)}{r(t)^3} \right\rangle \frac{z_0}{{r_0}^3}. \tag{6}$$

Here the sum is a sum over species, $N_j \gg 1$ is the number of particles in species j, V is the system volume, $\mathbf{r}(t) = (x(t), y(t), z(t))$ is the relative position of the particles with relative initial position $\mathbf{r}_0 = (x_0, y_0, z_0)$, and $\mathrm{v}_z(t)$ is their relative parallel velocity. The function $f_{ij}(v_{z_0})$ is the distribution of the initial relative velocity v_{z_0} (normalized to unity), assumed to be Maxwellian with temperature T, and the remaining average $\langle\cdot\rangle$ is over the initial positions and velocities of the other $N-2$ charges.

Finally, we will find it useful to write Eq. (6) as

$$D_i = \sum_j \left(\frac{e_i e_j}{m_i}\right) n_j \int d^3 r_0 \int dv_{z_0} f_{ij}(v_{z_0}) \langle \Delta \mathrm{v}_{ij} \rangle \frac{z_0}{{r_0}^3}, \tag{7}$$

where n_j is the density of species j, and $\langle \Delta \mathrm{v}_{ij} \rangle$ is the velocity kick given to particle i due to its interaction with particle j averaged over initial coordinates of the other $N-2$ charges,

$$\langle \Delta \mathrm{v}_{ij} \rangle \equiv \frac{e_i e_j}{m_i} \int_0^\infty dt \left\langle \frac{z(t)}{r(t)^3} \right\rangle . \tag{8}$$

III. EVALUATION OF D USING INTEGRATION ALONG UNPERTURBED ORBITS

Both the FP and Boltzmann approaches can be used to evaluate the required integrals in Eqs. (7) and (8), but each approach is, by itself, inadequate. In the simplest version of FP theory, one assumes that particle-particle interactions have only a small effect, so that one can use unperturbed orbits: $z(t) = z_0 + \mathrm{v}_{z_0} t$, $x(t) = x_0$, $y(t) = y_0$. Substituting these orbits in Eq. (8) and performing the time integral yields the following expression for the velocity kick $\Delta \mathrm{v}_{ij}$, provided that v_{z_0} is nonzero:

$$\Delta \mathrm{v}_{ij}^{\mathrm{IUO}} = \frac{e_i e_j / m_i}{\mathrm{v}_{z_0} r_0}, \quad \mathrm{v}_{z_0} \neq 0 \, . \tag{9}$$

However, this expression is odd in v_{z_0} and even in z_0, so it clearly yields zero when integrated over v_{z_0} and z_0 in Eq. (7). In IUO, the diffusion is due only to particles with initial relative velocity $\mathrm{v}_{z_0} = 0$, i.e. a resonant interaction that lasts for a long time.

A slightly more sophisticated approach must be employed to evaluate the velocity kick in this case. Equation (8) can be expressed in terms of the Fourier transform of the interaction,

$$\Delta \mathrm{v}_{ij} = -\frac{e_i e_j}{m_i} \int_0^\infty dt \int \frac{d^3 k}{(2\pi)^3} \frac{4\pi i k_z}{k^2} e^{i \mathbf{k} \cdot \mathbf{r}(t)} \, . \tag{10}$$

Performing the time integral using the unperturbed orbits yields

$$\Delta \mathrm{v}_{ij}^{\mathrm{IUO}} = -\frac{e_i e_j}{m_i} \int \frac{d^3k}{(2\pi)^3} \frac{4\pi i k_z}{k^2} e^{i\mathbf{k}\cdot\mathbf{r}_0} \left(\pi\delta(k_z \mathrm{v}_{z_0}) + \frac{iP}{k_z \mathrm{v}_{z_0}} \right) , \tag{11}$$

where P stands for the principal part of the expression. The first term in the bracket in Eq. (11) is due to resonant interactions, which were not accounted for previously. Performing the wavenumber integrals yields

$$\Delta \mathrm{v}_{ij}^{\mathrm{IUO}} = \frac{e_i e_j}{m_i} \left(2\delta(\mathrm{v}_{z_0}) \frac{\sinh^{-1}(z_0/\rho)}{r_0} + \frac{P}{\mathrm{v}_{z_0} r_0} \right) . \tag{12}$$

where $\rho = \sqrt{x_0^2 + y_0^2}$ is the impact parameter of the collision. The first term in the bracket in Eq. (12) is the required form of the velocity kick due to resonant interactions, while the second term is the same as Eq. (9). Only the first term, even in v_{z_0} and odd in z_0, contributes to the integrand in Eq. (7) which is also even in v_{z_0} and odd in z_0.

When Eq. (12) is employed in Eq. (7) and the integrals over z_0 and v_{z_0} are performed, we are left with a logarithmically-divergent integral over impact parameter:

$$D_i^{\mathrm{IUO}} = \sum_j 2 \left(\frac{e_i e_j}{m_i} \right)^2 n_j f_{ij}(0) \int 2\pi \, \frac{d\rho}{\rho} \tag{13}$$

where $f_{ij}(0) = 1/\sqrt{2\pi T/\mu}$. This result can also be obtained from the Rostoker collision operator[16] applied to plasmas with $r_c < \lambda_D$.[4] The divergences in the ρ integral are commonly dealt with by arguing that Debye shielding cuts off the interaction when $\rho > \lambda_D$. For the lower bound we note that interactions with $\rho < \mathrm{Max}(r_c, b)$ are not dealt with properly in IUO, where $b = |e_i e_j| / T$ is the distance of closest approach. This argument implies

$$D_i^{\mathrm{IUO}} = \sum_j 4\pi \left(\frac{e_i e_j}{m_i} \right)^2 n_j f_{ij}(0) \log(\lambda_D / \mathrm{Max}(b, r_c)) . \tag{14}$$

However, we will see that this result is incorrect, as it neglects the effects of Boltzmann collisions and caging.

IV. EVALUATION OF D USING BOLTZMANN COLLISIONS

The previous evaluation can be improved by using exact particle trajectories for the relative axial motion of the colliding pair, rather than IUO. However, we still neglect interactions

with the other $N-2$ charges, so we drop the average in Eq. (8). Energy conservation in such an isolated collision implies that the relative velocity must satisfy

$$\frac{1}{2}\mu \mathrm{v}_z^2 + \frac{e_i e_j}{\sqrt{\rho^2+z^2}} = \frac{1}{2}\mu \mathrm{v}_{z_0}^2 + \frac{e_i e_j}{\sqrt{\rho^2+z_0^2}}\,. \tag{15}$$

This implies that the final velocity ($z \to \pm\infty$) is given by

$$\mathrm{v}_{z_f} = \pm\sqrt{\mathrm{v}_{z_0}^2 + 2\frac{e_i e_j}{\mu\sqrt{\rho^2+z_0^2}}}\,. \tag{16}$$

The sign of v_{z_f} is determined by whether or not a reflection occurred. Reflections occur provided that particles are moving toward $z=0$ initially (i.e. $\mathrm{v}_{z_0} z_0 \le 0$), and that a turning point exists in the orbit; this requires

$$\frac{e_i e_j}{\rho} \ge \frac{1}{2}\mu \mathrm{v}_{z_0}^2 + \frac{e_i e_j}{r_0}\,. \tag{17}$$

The total change $\Delta\mathrm{v}$ in relative velocity in the collision is, therefore,

$$\Delta\mathrm{v} = s\sqrt{\mathrm{v}_{z_0}^2 + 2\frac{e_i e_j}{\mu\sqrt{\rho^2+z_0^2}}} - \mathrm{v}_{z_0}. \tag{18}$$

Here s is the sign of the final velocity, which equals the sign of the initial velocity when no reflection occurs, and is opposite in sign otherwise.

However, only that portion of $\Delta\mathrm{v}$ that is even in v_{z_0} enters into the diffusion coefficient, because f_{ij} is even in v_{z_0}. This even portion is nonzero only for speeds in the range given by Eq. (17) where reflection occurs, and is therefore given by

$$\Delta\mathrm{v}_{\mathrm{even}} = \begin{cases} \mathrm{Sign}(z_0)\sqrt{\mathrm{v}_{z_0}^2 + 2\frac{e_i e_j}{\mu r_0}}, & \mathrm{v}_{z_0}^2 \le \frac{2e_i e_j}{\mu}\left(\frac{1}{\rho}-\frac{1}{r_0}\right) \\ 0, & \text{otherwise} \end{cases}\,. \tag{19}$$

Note that this result vanishes for attractive interactions where no reflection occurs.* The velocity dependence of Eq. (19) replaces the delta function of Eq. (12), noting that momentum conservation implies that the above change in relative velocity is related to the change in the velocity of particle i through $\Delta\mathrm{v}_{ij\,\mathrm{even}} = \mu\Delta\mathrm{v}_{\mathrm{even}}/m_i$.

*For attractive interactions, particles form bound pairs if their relative energy is less than zero ("guiding-center atoms"[17]). For such particle pairs $\Delta\mathrm{v}_{\mathrm{even}}$ is undefined since v_z oscillates with time. The time average of these oscillations yields $\Delta\mathrm{v}_{\mathrm{even}} = 0$, so, for the purposes of computing the diffusion coefficient, Eq. (19) is also correct for negative energies. Simply put, bound pairs do not contribute to velocity diffusion in Boltzmann theory.

The integrals over z_0 and v_{z_0} in Eq. (7) can then be easily carried out. At this point it is useful to scale the variables. We will scale positions by impact parameter ρ : $\overline{\mathbf{r}} \equiv \mathbf{r}/\rho$; and times by $t_B = (\mu\rho^3/|e_i e_j|)^{1/2}$: $\bar{t} \equiv t/t_B$. Thus, velocities are scaled by $\rho/t_B = \sqrt{|e_i e_j|/\mu\rho}$; $\overline{\mathrm{v}}_{z_0} \equiv \mathrm{v}_{z_0}/\sqrt{|e_i e_j|/\mu\rho}$.

We can simplify Eq. (7) by noting that the scaled velocities that contribute to the integrand in Eq. (7) are of order unity [see Eq. (19)], and such velocities are small compared to the relative thermal speed $\sqrt{T/\mu}$ provided that impact parameters satisfy $\rho > b$. We can therefore replace $f_{ij}(\mathrm{v}_{z_0})$ by $f_{ij}(0)$ in Eq. (7).

In these scaled variables, Eq. (7) becomes

$$D_i^B = \sum_j \left(\frac{e_i e_j}{m_i}\right)^2 \mathrm{Sign}(e_i e_j) n_j f_{ij}(0) \int \frac{2\pi d\rho}{\rho} \int_{-\infty}^{\infty} d\overline{\mathrm{v}}_{z_0} \int_{-\infty}^{\infty} d\overline{z}_0 \frac{\overline{z}_0}{(1+\overline{z}_0^2)^{3/2}} \Delta\overline{\mathrm{v}}_{\mathrm{even}}\,, \tag{20}$$

where $\Delta\overline{\mathrm{v}}_{\mathrm{even}} = \Delta\mathrm{v}_{\mathrm{even}}/\sqrt{e_i e_j/\mu\rho}$. Using Eq. (19) it is not difficult to show that this function is independent of ρ, so that $\Delta\overline{\mathrm{v}}_{\mathrm{even}} = \Delta\overline{\mathrm{v}}_{\mathrm{even}}(\overline{z}_0, |\overline{\mathrm{v}}_{z_0}|)$. Then the required integral over $\overline{z}_0$ in Eq. (20) is a function only of $|\overline{\mathrm{v}}_{z_0}|$, which we denote by $\overline{g}(|\overline{\mathrm{v}}_{z_0}|)$:

$$\bar{g}(|\bar{\mathrm{v}}_{z_0}|) \equiv \mathrm{Sign}(e_i e_j) \int d\overline{z}_0 \frac{\overline{z}_0}{(1+z_0^2)^{3/2}} \Delta\bar{\mathrm{v}}_{\mathrm{even}}. \tag{21}$$

For attractive interactions, $\overline{g} = 0$, while for repulsive interactions, substitution of Eq. (19) for $\Delta\mathrm{v}_{\mathrm{even}}$ yields

$$\bar{g}(|\bar{\mathrm{v}}_{z_0}|) = \begin{cases} \frac{2}{3}\left(2^{3/2} - |\bar{\mathrm{v}}_{z_0}|^3\right), & |\bar{\mathrm{v}}_{z_0}| \le \sqrt{2} \\ 0, & |\bar{\mathrm{v}}_{z_0}| \ge \sqrt{2} \end{cases}. \tag{22}$$

This function of velocity is plotted in Fig. 2. Integrating $\overline{g}$ over scaled velocity then yields a factor of 4, which when used in Eq. (20) implies

$$D_{i\ \mathrm{Boltzmann}} = \begin{cases} \sum_j 4\left(\frac{e_i e_j}{m_i}\right)^2 n_j f_{ij}(0) \int 2\pi \frac{d\rho}{\rho}, & e_i e_j > 0 \\ 0, & e_i e_j < 0 \end{cases}. \tag{23}$$

For a repulsive interaction this result is a factor of two larger than the IUO calculation of Eq. (13), while for an attractive interaction there is no diffusion at all in Boltzmann theory. The discrepancy between Boltzmann and FP theory for repulsive interactions was also derived, but not resolved, in Ref. 4.

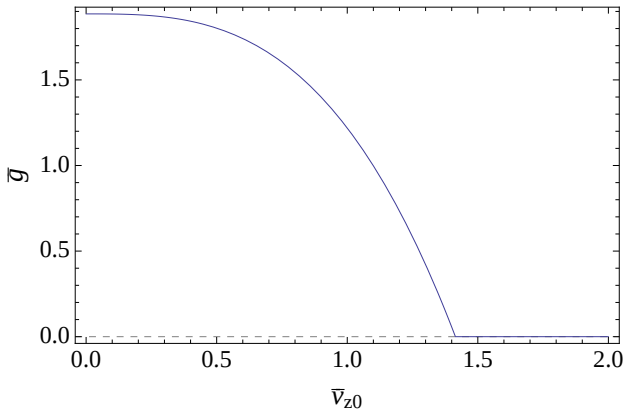

FIG. 2. The function $\bar{g}$, plotted versus scaled velocity $\bar{v}_{z_0}$, for repulsive Boltzmann collisions (solid line; see Eq. (22)) and attractive Boltzman collisions (dashed line).

V. EVALUATION OF D USING A LANGEVIN MODEL. (1): ESTIMATE AND FOKKER-PLANCK THEORY

In order to resolve the apparent contradiction between the Boltzmann result of Eq. (23) and the FP/IUO result of Eq. (13), we must take into account that these results apply only for certain ranges of the impact parameter ρ: FP theory works only for $\rho > d$ and the Boltzmann result (modified by collisional caging) works only for $\rho < d$. Collisions with impact parameters $\rho < d$ occur sufficiently rapidly that they can be regarded as isolated events well-described by Boltzmann theory; but collisions with $\rho > d$ happen so slowly that velocity diffusion dominates the particle orbits.

This intuition suggests that the diffusion coefficient due to long-range collisions is given by a sum of the Boltzmann result, evaluated for impact parameters $\rho < d$, and the FP result, evaluated for $\rho > d$. Using Eqs. (13) and (23) then yields the preliminary estimate

$$D_i = \sum_j \left(\frac{e_i e_j}{m_i}\right)^2 n_j f_{ij}(0) 2\pi \left[\left\{ \begin{array}{l} 4, \ e_i e_j > 0 \\ 0, \ e_i e_j < 0 \end{array} \right\} \int_{\max(b, r_c)}^{d} \frac{d\rho}{\rho} + 2 \int_d^{\lambda_D} \frac{d\rho}{\rho} \right]. \tag{24}$$

The first term is the Boltzmann contribution, and the second is the FP contribution. The cutoffs on the integrals assume that $r_c < d$; otherwise there is no Boltzmann contribution and the FP integration runs from r_c to λ_D. This can be accounted for by replacing d by $max\,(d,\ r_c)$. We will see in section IX that the functional form of Eq. (24) is correct, but the Boltzmann coefficient of 4 for $e_i e_j > 0$ is enhanced by collisional caging.

In order to test this intuition we introduce the following Langevin-type equation of motion for the relative position, written in scaled variables as

$$\frac{d^2\bar{z}}{d\bar{t}^2} = \mathrm{Sign}(e_i e_j)\frac{\bar{z}}{(1+\bar{z}^2)^{3/2}} + \bar{\tilde{a}} \tag{25}$$

where $\bar{\tilde{a}}$ is a (scaled) stochastic acceleration modeling the interaction of the colliding pair with surrounding plasma particles. This acceleration has zero mean and has an autocorrelation function whose time integral is given by the velocity diffusion itself:

$$2\bar{D} = \int_{-\infty}^{\infty} d\bar{t}\,\langle \bar{\tilde{a}}(t)\bar{\tilde{a}}(0)\rangle \tag{26}$$

where $D = D_i + D_j$ is the diffusion coefficient for the relative velocity of particles i and j.

Langevin models often include a term $-\nu\dot{z}$ due to the mean slowing down, but we drop this term in Eq. (25) as it is negligible compared to the terms kept. This $-\nu\dot{z}$ term would change velocities in a time of order $1/\nu$, but we will see that this time is much longer than the collisional correlation time $t_{\max}$.

In scaled variables the diffusion coefficient is related to the scale length d through

$$\bar{D} = Dt_B^3/\rho^2 = (\rho/d)^{5/2}\,. \tag{27}$$

With this scaling the diffusion coefficient as given by Eq. (20) can be written as

$$D_i = \sum_j \left(\frac{e_i e_j}{m_i}\right)^2 n_j f_{ij}(0) \int 2\pi \frac{d\rho}{\rho}\bar{h}([\rho/d]^{5/2})\,, \tag{28}$$

where we have used Eq. (27) to write $\bar{D}$ in terms of ρ, and the function $\bar{h}(\bar{D})$ is defined as

$$\bar{h}(\bar{D}) = 2\int_0^{\infty} d\bar{\mathrm{v}}_{z_0}\bar{g}(|\bar{\mathrm{v}}_{z_0}|,\bar{D})\,. \tag{29}$$

Here $\bar{g}$ is the generalization of Eq. (21) to finite $\bar{D}$, given by

$$\bar{g}(|\bar{\mathrm{v}}_{z_0}|,\bar{D}) \equiv \mathrm{Sign}(e_i e_j)\int d\bar{z}_0 \frac{\bar{z}_0}{(1+\bar{z}_0^2)^{3/2}}\langle\Delta\bar{\mathrm{v}}\rangle_{even}, \tag{30}$$

and $\langle\Delta\bar{\mathrm{v}}\rangle \equiv \langle\bar{\mathrm{v}}_z(\bar{t}\to\infty)\rangle - \bar{\mathrm{v}}_{z_0}$ is obtained by a solution of Eq. (25) with scaled initial conditions $\bar{z}(0) = \bar{z}_0$, $\bar{\mathrm{v}}_z(0) = \bar{\mathrm{v}}_{z_0}$. The average is over an ensemble of realizations of the stochastic acceleration. Note that $\langle\Delta\bar{\mathrm{v}}\rangle = \langle\Delta\bar{\mathrm{v}}\rangle(\bar{z}_0,\bar{\mathrm{v}}_{z_0},\bar{D})$, with all dependence on ρ

scaled out, and dependence on the scaled diffusion coefficient through Eq. (26). Of course, $\langle \Delta \overline{\mathrm{v}}_{\mathrm{even}} \rangle = \frac{1}{2}[\langle \Delta \overline{\mathrm{v}} \rangle(\overline{z}_0, \overline{\mathrm{v}}_{z_0}, \overline{D}) + \langle \Delta \overline{\mathrm{v}} \rangle(\overline{z}_0, -\overline{\mathrm{v}}_{z_0}, \overline{D})]$.

When $\rho \ll d$, Eq. (27) implies that $\bar{D} \to 0$, and we (might hope to) neglect the stochastic acceleration in Eq. (25). In this case we might expect to obtain the Boltzmann result for the function $\bar{g}$, given by Eq. (22) and shown in Fig. 2, and hence obtain the Boltzmann result for D_i, Eq. (23). However, we will see that in fact the stochastic acceleration term cannot be neglected even when $\bar{D} \to 0$ because of collisional caging effects.

On the other hand, when $\rho \gg d$ we have $\bar{D} \gg 1$, so the stochastic acceleration overwhelms the Coulomb interaction and the equation of motion simplifies to

$$\frac{d^2 \bar{z}}{d\bar{t}^2} = \bar{\bar{a}} \, . \tag{31}$$

This is diffusion-broadened IUO, a form of Fokker-Planck (FP) theory. This limit can be solved analytically. Using this equation of motion in Eq. (10) and performing the average (see Ref. 10) yields

$$\langle \Delta \bar{\mathrm{v}} \rangle^{\mathrm{FP}} = -\mathrm{Sign}(e_i e_j) \int \frac{d^3k}{(2\pi)^3} \frac{4\pi i k_z}{k^2} e^{i\mathbf{k}\cdot\bar{\mathbf{r}}_0} \int_0^\infty d\bar{t} e^{ik_z \bar{\mathrm{v}}_{z_0} \bar{t} - \frac{1}{3} k_z^2 \bar{D} \bar{t}^3} \, . \tag{32}$$

Applying this FP result to Eq. (30), we find that the function $\bar{g}$ can be written as

$$\bar{g}^{\mathrm{FP}}(\overline{\mathrm{v}}_{z_0}, \overline{D}) = \frac{2}{\bar{D}^{\,1/3}} \gamma(\bar{\mathrm{v}}_{z_0} / \bar{D}^{1/3}) \, , \quad \bar{D} \gg 1 \tag{33}$$

where the function $\gamma(x)$ is defined as

$$\gamma(x) = \frac{2}{\pi |x|} \int_0^\infty dk_z k_z K_0^2(k_z) \int_0^\infty du \, \cos u \, \exp\left[-\frac{u^3}{3k_z |x|^3} \right] \tag{34}$$

and where $K_0(k)$ is a modified Bessel function of the second kind. The function $\gamma(x)$ is plotted in Fig 3. It is peaked around $x = 0$. By direct integration, the area under this function can be easily shown to be equal to unity. Thus, $\bar{g}^{FP}$ is a function of scaled velocity whose width is of order $\bar{D}^{1/3}$. This function replaces the delta function in Eq. (12).

Now, in writing Eq. (28), we implicitly assumed that the velocity width of $\overline{g}$ is small compared to the thermal speed so that we could replace $f_{ij}(\mathrm{v}_{z_0})$ by $f_{ij}(0)$. We saw this was true in the Boltzmann theory for $\overline{g}$ [Eq. (22)] and we must now check to see whether this is still true in the FP regime $\overline{D} \gg 1$.

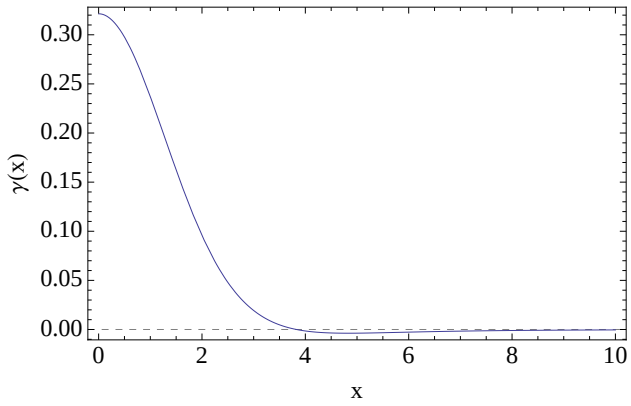

FIG. 3. The diffusion-broadened δ-function $\gamma(x)$.

The velocity width of $\overline{g}^{FP}$ in unscaled units is $\rho/t_B\,\overline{D}^{1/3} = (\rho D)^{1/3}$. This width is small compared to the thermal speed $\sqrt{T/\mu}$ provided that $\rho \ll \lambda_D/\Gamma^{3/2}$, which is true for all $\rho < \lambda_D$. Here, $\Gamma \equiv e^2/aT$ is the Coulomb coupling parameter, where a is the mean inter particle spacing (Wigner-Seitz radius). In a weakly coupled plasma, $\Gamma \ll 1$. Thus, even in the FP regime $\overline{D} \gg 1$, it is safe to replace $f_{ij}(\mathrm{v}_{z_0})$ by $f_{ij}(0)$ in Eq. (28).

Since the area under the function $\gamma(x)$ equals one, Eqs. (29) and (33) imply that $\bar{h}^{\mathrm{FP}} = 2$. This in turn implies that the FP result for the diffusion coefficient is still given by the IUO form, Eq. (13). This is because the velocity width $(\rho D)^{1/3}$ of $\overline{g}$ in the FP regime is small compared to the thermal speed, so we can approximate $\overline{g}^{\mathrm{FP}}$ by a δ-function, as was done in IUO.

We expect that this FP result will be valid provided that the width in (scaled) velocity of the function $\bar{g}$ is much greater than one, so that its width is much larger than the width of the equivalent function given in Eq. (22) due to Boltzmann reflections. Since the scaled velocity width of $\bar{g}^{FP}$ is $\bar{D}^{\,1/3}$, we require $\bar{D} >> 1$ for the FP approximation to be valid. This is consistent with the initial approximation in our analysis, Eq. (31), where we dropped the Coulomb interaction in the equation of motion.

VI. EVALUATION OF D USING A LANGEVIN MODEL. (2): MONTE-CARLO METHOD

We have numerically evaluated the functions $\bar{g}$ and $\bar{h}$ using a Monte-Carlo method. Equation (25) is finite-differenced using the second-order leapfrog method,

$$\begin{aligned} \bar{z}_n &= \bar{z}_{n-1} + \Delta\bar{t}\,\bar{\mathrm{v}}_{n-1/2}\,, \\ \bar{\mathrm{v}}_{n+1/2} &= \bar{\mathrm{v}}_{n-1/2} \pm \Delta\bar{t}\frac{\bar{z}_n}{(1+\bar{z}_n^2)^{3/2}} + \tilde{\mathrm{v}}_n, \end{aligned} \tag{35}$$

where $\tilde{\mathrm{v}}_n$ is a random real number uniformly distributed in the range $(-\sqrt{6\bar{D}\Delta\bar{t}}, \sqrt{6\bar{D}\Delta\bar{t}})$. This range is chosen so that $\langle\tilde{\mathrm{v}}_n^2\rangle = 2\overline{D}\Delta\bar{t}$. For given values of the initial position $\bar{z}_0$ and speed $|\bar{\mathrm{v}}_{z_0}|$ the equations are integrated twice, with positive and negative initial velocities, and the result for $\Delta\overline{\mathrm{v}} = \overline{\mathrm{v}}_{z_f} - \overline{\mathrm{v}}_{z_0}$ is averaged to obtain $\Delta\overline{\mathrm{v}}_{\mathrm{even}}$, where $\overline{\mathrm{v}}_{z_f}$ is the final velocity in the simulation. This result is then averaged over many runs with different realizations of $\tilde{\mathrm{v}}_n$ in order to obtain $\langle\Delta\overline{\mathrm{v}}\rangle_{\mathrm{even}}$. Of course, we cannot take the limit as $\bar{t} \to \infty$ when determining the final velocity, but we take a sufficiently large value of $\bar{t}$ so that the results for $\langle\Delta\overline{\mathrm{v}}\rangle_{\mathrm{even}}$ are independent of the value of $\bar{t}$. The maximum value of $\bar{t}$ used, $\bar{t}_{\mathrm{max}}$, depends on the value of $\bar{D}$ (more on this later).

The function $\bar{g}$ is also determined using a Monte-Carlo approach. The integral over $\bar{z}_0$ in Eq. (30) is performed by first transforming variables from $\bar{z}_0$ to s, where $0 < s < 1$. The transformation is

$$\bar{z}_0 = \frac{\sqrt{s(2-s)}}{1-s}\,. \tag{36}$$

With this transformation we may write Eq. (30) as

$$\bar{g}(|\bar{\mathrm{v}}_{z_0}|, \bar{D}) \equiv 2\,\mathrm{Sign}(e_i e_j) \int_0^1 ds\,\langle\Delta\bar{\mathrm{v}}\rangle_{\mathrm{even}}\,. \tag{37}$$

We then evaluate the integral by choosing many random values of s uniformly distributed on the interval (0,1) and taking the mean value of $\langle\Delta\bar{\mathrm{v}}\rangle_{\mathrm{even}}$ over these values of s.

Results for $\bar{g}$ are shown for $\bar{D} = 3.2$ in Fig. 4. There is some scatter in the results at each $\bar{\mathrm{v}}_{z_0}$ value shown because of statistical noise in the Monte Carlo method. However, one can see that for both attractive and repulsive forms of the interaction, the result is close to the FP theory, given by Eq. (33), shown by the solid curve in the figure. This is because $\bar{D} = 3.2$ is sufficiently large so that most particles diffuse in velocity before they can reflect (or pass by in the case of an attractive interaction).

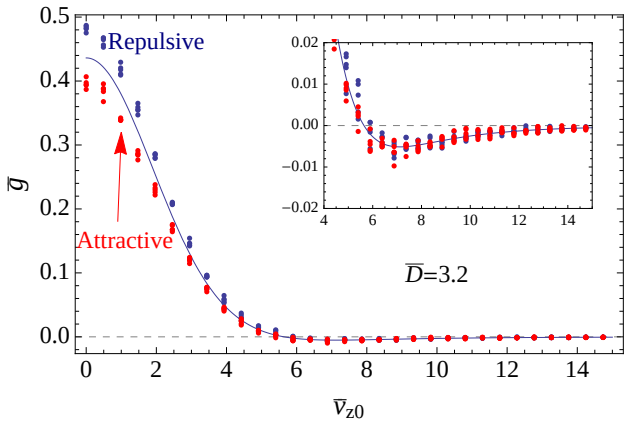

FIG. 4. The function $\bar{g}$, plotted versus scaled velocity $\bar{v}_{z_0}$, for scaled diffusion coefficient $\bar{D} = 3.2$. The solid line is the FP theory, given by Eq. (33). Blue dots and red dots are Monte-Carlo evaluations of the function, for repulsive and attractive Coulomb interactions respectively. There are 5 evaluations for each velocity. The inset is an expanded view for $v_{z_0} > 4$.

However, for smaller $\bar{D}$ values the Monte Carlo values for $\bar{g}$ diverge from the FP theory. In Fig. 5 results for $\bar{g}$ are displayed for $\bar{D} = 0.1$. The Monte-Carlo results for attractive interactions are considerably smaller than FP theory, given by the solid line, while the results for repulsive interactions are considerably larger. For comparison, the dotted lines show the Boltzmann theory for $\bar{g}$, which also do not bear much resemblance to the Monte-Carlo results.

The area $\bar{h} = \int_{-\infty}^{\infty} d\bar{v}_{z_0} \bar{g}$ under these curves is displayed in Fig 6 versus $\bar{D}$. The upper dots are Monte-Carlo evaluations for repulsive interactions, and the lower dots are for attractive interactions. Integration over initial velocities in Eq. (29) is performed by MC sampling over a range $|\bar{v}_{z_0}| < v_{max}$, where v_{max} depends on $\overline{D}$. For $\overline{D} = 10^{-3}$, $v_{max} = 1.5$ is sufficient, but for larger $\overline{D}$ v_{max} must be increased as $\overline{g}(\bar{v}_{z_0})$ broadens (see Figs. 4 and 5). For large $\bar{D}$ values the results converge toward $\bar{h} = 2$, as expected for FP theory. For small $\bar{D}$ values Monte-Carlo results for an attractive interaction approach zero, as expected for Boltzmann theory; but for repulsive interactions the results are larger than the $\bar{h} = 4$ value expected for repulsive Boltzmann collisions [see Eq. (23)].

This discrepancy is due to collisional caging. To probe this effect, we evaluated $\bar{h}$ for a range of values of the maximum time $\bar{t}_{max}$ used in the numerical integration of Eqs. (35). As shown in Fig. 7, for $1 << \bar{t}_{max} << 1/\bar{D}$, the value of $\bar{h}$ approaches the Boltzmann

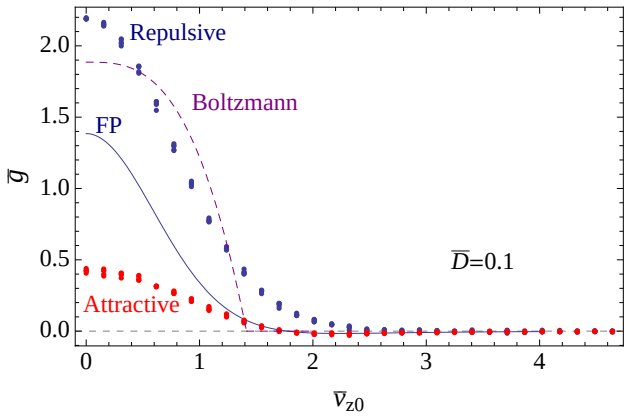

FIG. 5. The function $\bar{g}$, plotted versus scaled velocity $\bar{v}_{z_0}$, for scaled diffusion coefficient $\bar{D} = 0.1$. The solid line is the FP theory, given by Eq. (33). The dashed line is the Boltzmann theory for repulsive interactions (from Fig. 2). Blue dots and red dots are Monte-Carlo evaluations of the function, for repulsive and attractive Coulomb interactions respectively. There are 5 evaluations for each velocity.

result, $\bar{h} = 4$. However, for $\bar{t}_{\max} > 1/\bar{D}$, the value of $\bar{h}$ increases and converges to a new value $\bar{h} \approx 5.9$, the value plotted in Fig. 6. For $\bar{t}_{\max} > 1/\bar{D}$ particles have time to reverse their relative velocity due to diffusion, and collide again. If particles have sufficiently low relative velocity, they can reflect off one another several times consecutively. Each consecutive reflection produces the same sign of acceleration in Eq. (8), adding to Δv on each reflection, increasing the correlation time, and increasing the diffusion coefficient. As time goes on, two particles return to interact again and again since their motion is limited to one spatial dimension, so one might wonder why a finite result for Δv is obtained. Eventually, however (also on a time of order $1/\overline{D}$) velocity diffusion causes the relative velocity to become sufficiently large so that particles can pass by rather than reflect, after which the acceleration due to their interaction averages to zero. If through velocity diffusion they lose relative velocity and become reflecting again, it is equally likely for them to reflect from either side of their mutual center of mass, so the contribution to Δv of these later interactions also averages to zero.

As an aside, note that $\bar{t}_{\max} \sim 1/\overline{D}$ implies that $\nu\, t_{\max} \sim b/\rho$, so this justifies our having dropped the $\nu\dot{z}$ term in Langevin equation (25), provided $\rho \gg b$.

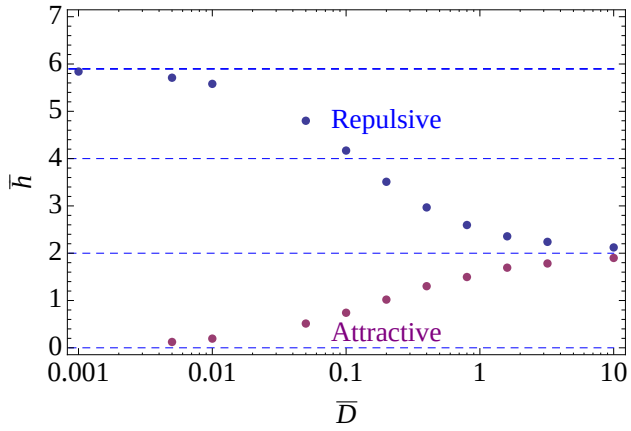

FIG. 6. Monte-Carlo evaluations of $\bar{h}$ plotted versus the scaled diffusion coefficient $\bar{D}$ for both repulsive and attractive Coulomb interactions. The dashed horizontal line at $\bar{h} = 2$ gives the FP result, while the lines at 0 and 4 give the Boltzmann theory for attractive and repulsive interactions respectively, and the line at 5.899 is the $D \to 0^+$ repulsive result enhanced by collisional caging (see Secs. VII and VIII).

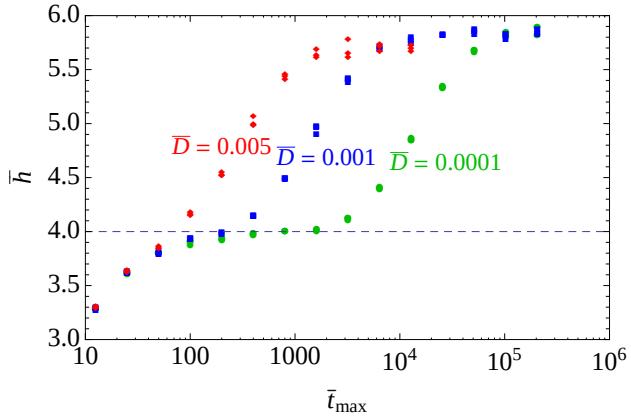

FIG. 7. Monte-Carlo evaluations of $\bar{h}$ evaluated for a range of maximum times, and for three values of $\bar{D}$. There are 3 evaluations shown for each $\overline{D}$ and $\bar{t}_{\rm max}$ value.

VII. EVALUATION OF D USING A LANGEVIN MODEL. (3): $\overline{D} \to 0^+$ LIMIT

For very small $\bar{D}$, one must take $\bar{t}_{\rm max}$ very large in the Monte-Carlo evaluation in order to capture the collisional caging effect, and this makes the numerical evaluation inefficient. It is therefore useful to rescale time and position in the following manner: $\hat{t} = t/t_0$, $\hat{z} = z/z_0$,

where $t_0 = e_i e_j/(\mu\rho D)$ and $z_0 = t_0 \mathrm{v}_0$, with $\mathrm{v}_0 \equiv \sqrt{e_i e_j/\mu\rho}$. In these scaled coordinates Eqs. (25) and (26) become

$$\frac{d^2\hat{z}}{d\hat{t}^2} = \frac{\rho D}{\mathrm{v}_0^3}\frac{\hat{z}}{(1+\hat{z}^2)^{3/2}} + \hat{\tilde{a}}, \tag{38}$$

$$\int_{-\infty}^{\infty} d\hat{t}\left\langle \hat{\tilde{a}}(t)\hat{\tilde{a}}(0)\right\rangle = 2\,. \tag{39}$$

As $D \to 0^+$, the Coulomb-interaction term can be neglected in Eq. (38) except for reflecting particles at $\hat{z} = 0$, which have scaled velocities in the range $|\hat{\mathrm{v}}_z| < \sqrt{2}$. Thus, the equation of motion becomes the same as in FP theory,

$$\frac{d^2\hat{z}}{d\hat{t}^2} = \hat{\tilde{a}} + A(\hat{z}, \hat{\mathrm{v}}_z)\,, \tag{40}$$

except that particles reflect at $\hat{z} = 0$ if they are in the velocity range $|\hat{\mathrm{v}}_z| < \sqrt{2}$: the reflector acceleration A is

$$A(\hat{z}, \hat{\mathrm{v}}_z) = -2\hat{\mathrm{v}}_z^2\,\mathrm{Sign}(\hat{\mathrm{v}}_z)H(\sqrt{2} - |\hat{\mathrm{v}}_z|)\delta(\hat{z})\,, \tag{41}$$

where $H(x)$ is the Heaviside step function. Particles that encounter the reflector receive an impulse $\int dtA = -2\hat{\mathrm{v}}_z$ sufficient to reflect their velocity. Note that Eqs. (39)–(41) are independent of $\overline{D}$.

We may then evaluate $\bar{g}$ and $\bar{h}$ via the Monte-Carlo method by choosing initial conditions $\bar{\mathrm{v}}_{z_0}$ and $\bar{z}_0$ as we did previously, determining the change in relative velocity $\Delta\bar{\mathrm{v}}$ using Eq. (18) as the particles escape to infinity, then rescaling coordinates and time and integrating the equations of motion using Eq. (40). Under this rescaling, the new "initial" position is $\hat{z}_0 = 0$, and the new "initial" velocity is $\hat{\mathrm{v}}_{z_0} = \bar{\mathrm{v}}_{z_0} + \Delta\bar{\mathrm{v}}$. More precisely, particles with $\hat{\mathrm{v}}_{z_0} < 0$ have $\hat{z}_0 = 0^-$ and particles with $\hat{\mathrm{v}}_{z_0} > 0$ have $\hat{z}_0 = 0^+$.

The result of the Monte-Carlo evaluation of $\bar{g}$ using this method is shown in Fig. 8 for $\hat{t}_{\max} = 0^+$ and $\hat{t}_{\max} = 64$. For $\hat{t}_{\max} = 0^+$, the result for $\bar{g}$ matches what is expected in Boltzmann theory (the solid line). However, for large $\hat{t}_{\max}$ the result is enhanced by collisional caging. In the Monte-Carlo simulation particles are observed to return and reflect several times, adding to the overall relative velocity change. The value $\hat{t}_{\max} = 64$ is sufficiently large so that the result for $\bar{g}$ is independent of further increases in $\hat{t}_{\max}$. A polynomial fit to the Monte-Carlo evaluations, of the form

$$\bar{g} = \begin{cases} a_0 + a_2\bar{\mathrm{v}}_{z_0}^2 + a_3|\bar{\mathrm{v}}|_{z_0}^3\,, & |\bar{\mathrm{v}}_{z_0}| < \sqrt{2} \\ 0, & |\bar{\mathrm{v}}_{z_0}| > \sqrt{2} \end{cases} \tag{42}$$

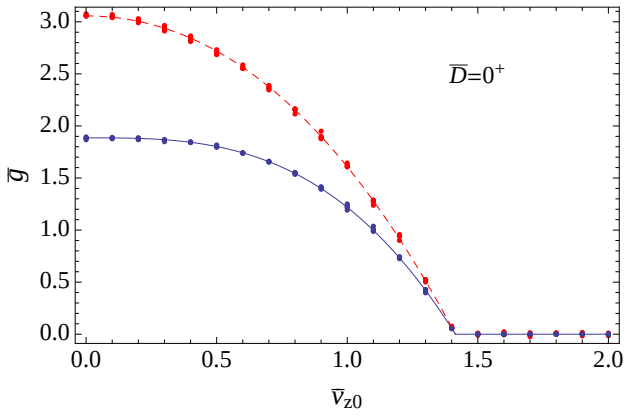

FIG. 8. The function $\bar{g}$ plotted versus scaled velocity $\bar{v}_{z_0}$, for repulsive interactions and for scaled diffusion coefficient $\bar{D} = 0^+$. Solid line: Boltzmann theory (see Eq.(22) and Fig. 2). Dashed line: Eq. (42). Dots: Monte-Carlo evaluations for $\hat{t}_{\max} = 0^+$ and $\hat{t}_{\max} = 64$. There are 5 Monte Carlo evaluations for each $\bar{v}_{z_0}$ value.

yields $a_0 = 3.056$, $a_2 = -1.254$, $a_3 = -0.1938$. This fit is constrained so that $\bar{g} = 0$ at $\bar{v}_{z_0} = \sqrt{2}$. The fit is displayed as the dashed curve in Fig. 8. Twice the area under this curve yields $\bar{h} = 5.894$ [see Eq. (29)]. Direct Monte-Carlo evaluations of $\bar{h}$, where $\bar{v}_{z_0}$ is chosen randomly rather than on a uniform grid, yield similar values, with an overall average value of $\bar{h}_+ = 5.899(1)$ (the + standing for repulsive interactions). This value is displayed in Fig. 6 as the upper dashed line. On the other hand, for attractive interactions, the corresponding value is $\bar{h}_- = 0$.

Some other statistical measures of the collisional caging can be extracted from the Monte-Carol simulation. If we choose particles in the simulation with initial velocities uniformly distributed in the range $-\sqrt{2} < \bar{v}_{z_0} < \sqrt{2}$, the fraction of particles that, after their first Boltzmann interaction, return with sufficiently low velocity to reflect at least once more, is 21.1%. The fraction of particles that return and reflect at least n_r times is shown versus n_r in Fig. 9. The line in the figure is a fit to the data of the form $a\,\exp(-b\,n_r)$ where $a = 0.35$ and $b = 0.9$.

Figure 10 shows the PDF of the time needed for a particle to complete one, two, or three reflections. For large times these PDFs show a scaling of roughly $\hat{t}_r^{-1.82}$ (the straight line on the log-log plot). This scaling of the PDF implies that the mean time needed to complete a given number of reflections is infinite. This same divergence also occurs for the first passage time in simple diffusion problems when a system boundary is at infinity, as is the case here.[20]

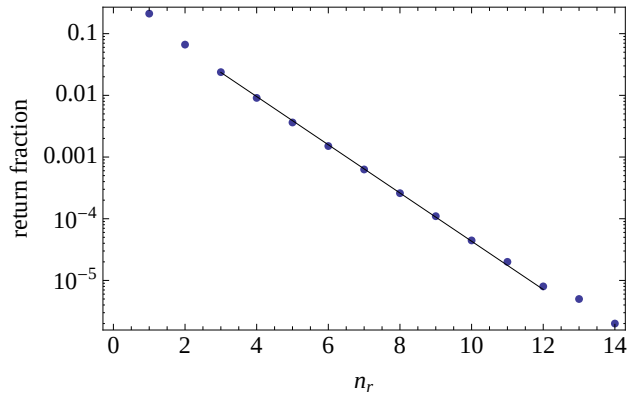

FIG. 9. Dots: Fraction of particles in the Monte Carlo simulation that return to reflect n_r or more times. The line is an exponential fit discussed in the text.

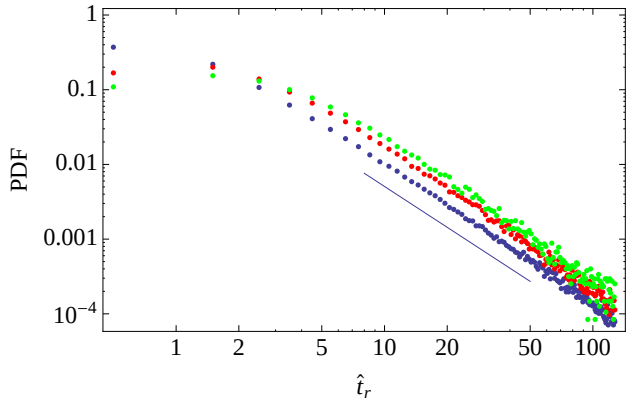

FIG. 10. Dots: Probability distribution function for the time needed to return and reflect 1 (blue), 2 (red), or 3 (green) times. The line is a power law fit to the slope of the curves discussed in the text.

This is because the particles can wander over large distances before returning to the reflector at $z = 0$.

VIII. A FOKKER-PLANCK SOLUTION OF THE $\overline{D} \to 0^+$ LIMIT

It is useful to note that the $\overline{D} \to 0^+$ Langevin model of the previous section maps on to a Fokker-Planck equation for the distribution function of a particle, $f(\hat{z}, \hat{\mathrm{v}}_z, \hat{t}; \hat{z}_0, \hat{\mathrm{v}}_{z_0})$:

$$\frac{\partial f}{\partial \hat{t}} + \hat{\mathrm{v}}_z \frac{\partial f}{\partial z} + A(\hat{z}, \hat{\mathrm{v}}_z) \frac{\partial f}{\partial \hat{\mathrm{v}}_z} = \frac{\partial^2 f}{\partial \hat{\mathrm{v}}_z^2} + \delta(\hat{t})\delta(\hat{z} - \hat{z}_0)\delta(\hat{\mathrm{v}}_z - \hat{\mathrm{v}}_{z_0}) \,, \tag{43}$$

where A is the acceleration due to the reflector, given by Eq. (41). We can relate f to the function $\overline{h}(\overline{D})$ required in the velocity diffusion coefficient [see Eq. (28)]. First, note that Eqs. (29) and (37) combine as

$$\overline{h} = 2 \int_{-\infty}^{\infty} d\overline{\mathrm{v}}_{z_0} \int_0^1 ds\, \Delta\overline{\mathrm{v}}(\overline{z}_0(s)\,, \overline{\mathrm{v}}_{z_0})\,. \tag{44}$$

Second, note that $\Delta\overline{\mathrm{v}}$ consists of two contributions in the limit $\bar{D} \to 0^+$, as discussed in the previous section. These are the contribution $\Delta\overline{\mathrm{v}}_B(\overline{z}_0, \overline{\mathrm{v}}_{z_0})$ from the first Boltzmann interaction with the force center in Eq. (25), and the contribution $\Delta\overline{\mathrm{v}}_c(\hat{z}_0, \hat{\mathrm{v}}_{z_0})$ from subsequent reflections as diffusing particles return, caused by collisional caging:

$$\Delta\overline{\mathrm{v}}(\overline{z}_0, \overline{\mathrm{v}}_{z_0}) = \Delta\overline{\mathrm{v}}_B(\overline{z}_0, \overline{\mathrm{v}}_{z_0}) + \Delta\mathrm{v}_c(\hat{z}_0, \hat{\mathrm{v}}_{z_0})\,. \tag{45}$$

Here $\hat{z}_0(\overline{z}_0, \overline{\mathrm{v}}_{z_0})$ is either 0^+ or 0^-, and $\hat{\mathrm{v}}_{z_0}$, the velocity after the first Boltzmann interaction, is given by Eq. (16):

$$\hat{z}_0 = \begin{cases} 0^+\,, & \overline{\mathrm{v}}_{z_0} > -\sqrt{2s} \\ 0^-\,, & \overline{\mathrm{v}}_{z_0} < -\sqrt{2s} \end{cases} \tag{46}$$

and

$$\hat{\mathrm{v}}_{z_0} = \sqrt{\overline{\mathrm{v}}_{z_0}^2 + 2 - 2s}\,\mathrm{Sign}\left(\overline{\mathrm{v}}_0 + \sqrt{2s}\right), \tag{47}$$

where we have applied Eq. (36) to write $\overline{z}_0$ in terms of s.

Now, the velocity step due to collisional caging is twice the time-integrated momentum flux onto the reflector at $\hat{z} = 0$, since each particle collision with the reflector causes a momentum change of $-2\hat{\mathrm{v}}_z$ to the particle. This implies

$$\begin{aligned} \Delta\overline{\mathrm{v}}_c = &\int_0^{\infty} d\hat{t} \int_{-\sqrt{2}}^{0} d\hat{\mathrm{v}}_z\, 2\hat{\mathrm{v}}_z^2 f(0^+, \hat{\mathrm{v}}_z, t; \hat{z}_0, \hat{\mathrm{v}}_{z_0}) \\ &+ \int_0^{\infty} d\hat{t} \int_0^{\sqrt{2}} d\hat{\mathrm{v}}_z\, 2\hat{\mathrm{v}}_z^2 f(0^-, \hat{\mathrm{v}}_z, t; \hat{z}_0, \hat{\mathrm{v}}_{z_0})\,. \end{aligned} \tag{48}$$

The first integral in Eq. (48) is the momentum flux onto the $\hat{z} = 0^+$ side of the reflector, and the second integral is the flux on the opposite side.

The velocity step $\Delta\mathrm{v}_B$ due to the first Boltzmann interaction was evaluated in Sec. IV,

as $\Delta\overline{\mathrm{v}}_B = \hat{\mathrm{v}}_{z_0} - \mathrm{v}_{z_0}$. The contribution $\overline{h}_B$ of $\Delta\overline{\mathrm{v}}_B$ to $\bar{h}_+ \equiv \lim_{\bar{D}\to 0^+}\bar{h}$ is

$$\begin{aligned}
\overline{h}_B &= 2\int_0^1 ds \int_{-\infty}^{\infty} d\overline{\mathrm{v}}_{z_0}\Delta\overline{\mathrm{v}}_B \\
&= 2\int_0^1 ds \int_0^{\infty} d\overline{\mathrm{v}}_{z_0}\sqrt{\overline{\mathrm{v}}_{z_0}^2 + 2 - 2s}\,\left[\mathrm{Sign}(\overline{\mathrm{v}}_{z_0} + \sqrt{2s}) + \mathrm{Sign}(-\overline{\mathrm{v}}_{z_0} + \sqrt{2s})\right] \\
&= 4\int_0^1 ds \int_0^{\sqrt{2s}} d\overline{\mathrm{v}}_{z_0}\sqrt{\overline{\mathrm{v}}_{z_0}^2 + 2 - 2s} \\
&= 4\,. \qquad (49)
\end{aligned}$$

This is the same result derived previously in Sec. IV.

The contribution $\overline{h}_c$ of $\Delta\overline{\mathrm{v}}_c$ to $\overline{h}_+$ is

$$\overline{h}_c = 2\int_0^1 ds \int_{-\infty}^{\infty} d\overline{\mathrm{v}}_{z_0}\,\Delta\overline{\mathrm{v}}_c(\hat{z}_0(\overline{z}_0, \overline{\mathrm{v}}_{z_0}),\, \hat{\mathrm{v}}_{z_0}(\overline{z}_0, \overline{\mathrm{v}}_{z_0}))\,. \qquad (50)$$

To simplify this expression, note that Eqs. (46) and (48) imply that $\hat{z}_0$ is a function of $\hat{\mathrm{v}}_{z_0}$ alone:

$$\hat{z}_0 = \begin{cases} 0^+\,, & \hat{\mathrm{v}}_{z_0} > 0 \\ 0^-\,, & \hat{\mathrm{v}}_{z_0} < 0 \end{cases} \qquad (51)$$

and therefore $\Delta\mathrm{v}_c = \Delta\overline{\mathrm{v}}_c(\hat{\mathrm{v}}_{z_0})$. Also, symmetry implies that

$$f(-\hat{z}, -\hat{\mathrm{v}}_z, \hat{t}; 0^-, -\hat{\mathrm{v}}_{z_0}) = f(\hat{z}, \hat{\mathrm{v}}_z, \hat{t}; 0^+, \hat{\mathrm{v}}_{z_0})\,, \qquad (52)$$

and this reflection symmetry, when applied to Eq. (48), implies $\Delta\mathrm{v}_c(\hat{\mathrm{v}}_{z_0}) = -\Delta\mathrm{v}_c(-\hat{\mathrm{v}}_{z_0})$. When this symmetry is applied to Eq. (50), we obtain

$$\overline{h}_c = 2\int_0^1 ds\, 2\int_0^{\sqrt{2s}} d\overline{\mathrm{v}}_{z_0}\Delta\overline{\mathrm{v}}_c(\hat{\mathrm{v}}_{z_0})\,, \qquad (53)$$

where we have used Eq. (47). Again applying Eq. (47) we can convert the integral over $\overline{\mathrm{v}}_{z_0}$ to one over $\hat{\mathrm{v}}_{z_0}$, obtaining

$$\overline{h}_c = 4\int_0^1 ds \int_{\sqrt{2-2s}}^{\sqrt{2}} d\hat{\mathrm{v}}_{z_0}\frac{\hat{\mathrm{v}}_{z_0}\Delta\overline{\mathrm{v}}_c(\hat{\mathrm{v}}_{z_0})}{\sqrt{\hat{\mathrm{v}}_{z_0}^2 + 2s - 2}}\,. \qquad (54)$$

The integral over s can also be performed, resulting in the simple expression

$$\overline{h}_c = 4 \int_0^{\sqrt{2}} d\hat{\mathrm{v}}_{z_0} \hat{\mathrm{v}}_{z_0}^2 \, \Delta\overline{\mathrm{v}}_c(\hat{\mathrm{v}}_{z_0}) \, . \tag{55}$$

Combining Eqs. (55), (48) and (49) then yields

$$\begin{aligned} \overline{h}_+ = 4 + 8 \int_{-\sqrt{2}}^{0} d\hat{\mathrm{v}}_z \hat{\mathrm{v}}_z^2 f_{\mathrm{eq}}(0^+, \hat{\mathrm{v}}_z) \\ -8 \int_0^{\sqrt{2}} d\hat{\mathrm{v}}_z \hat{\mathrm{v}}_z^2 f_{\mathrm{eq}}(0^-, \hat{\mathrm{v}}_z) \end{aligned} \tag{56}$$

where

$$f_{\mathrm{eq}}(\hat{z}, \hat{\mathrm{v}}_z) = \int_0^{\sqrt{2}} d\hat{\mathrm{v}}_{z_0} \hat{\mathrm{v}}_{z_0}^2 \int_0^{\infty} d\hat{t} \, f(\hat{z}, \hat{\mathrm{v}}_z, \hat{t}; 0^+, \hat{\mathrm{v}}_{z_0}) \tag{57}$$

is an equilibrium solution of the FP equation. This function satisfies the time and velocity integral of Eq. (43),

$$\hat{\mathrm{v}}_z \frac{\partial f_{\mathrm{eq}}}{\partial \hat{z}} + A(\hat{z}, \hat{\mathrm{v}}_z) \frac{\partial f_{\mathrm{eq}}}{\partial \hat{\mathrm{v}}_z} = \frac{\partial^2 f_{\mathrm{eq}}}{\partial \hat{\mathrm{v}}_z^2} + \delta(\hat{z} - 0^+) \hat{\mathrm{v}}_z^2 H(\hat{\mathrm{v}}_z) H(\sqrt{2} - \hat{\mathrm{v}}_z) \tag{58}$$

where $H(x)$ is the Heaviside step function.

We have solved Eq. (58) numerically using a non-uniform grid method. Details are in Appendix A. Figure 11 displays a contour plot of the solution near the reflector, shown as a red line at $z = 0$ for $|\hat{\mathrm{v}}_z| < \sqrt{2}$. There are discontinuities in the solution at the reflector ends, at $\hat{\mathrm{v}}_z = \pm\sqrt{2}$, caused by the difference between particles that pass and those that reflect. This difference produces rapid variation in the solution that is difficult to capture accurately in a numerical method. The discontinuities can be seen in Fig. 12, which shows the solution for f_{eq} along the front ($\hat{z} = 0^+$) and rear ($\hat{z} = 0^-$) faces of the reflector, and beyond.

On large scales, far from the origin, the presence of the reflector is unimportant and the solution approaches the equilibrium solution $f_{\mathrm{free}}(\hat{z}, \hat{\mathrm{v}}_z)$ of the FP equation with no boundaries or reflectors, which can be obtained from the free particle FP Green's function

$$\begin{aligned} G(\hat{z}, \hat{\mathrm{v}}_z, \hat{t}; \hat{z}_0, \hat{\mathrm{v}}_{z_0}) = \frac{\sqrt{3}}{2\pi\hat{t}^2} \\ e^{-\frac{3(\hat{z}-(\hat{z}_0+\hat{\mathrm{v}}_{z_0}\hat{t}))^2}{\hat{t}^3} + \frac{3(\hat{z}-(\hat{z}_0+\hat{\mathrm{v}}_{z_0}\hat{t}))(\hat{\mathrm{v}}_z-\hat{\mathrm{v}}_{z_0})}{\hat{t}^2} - \frac{(\hat{\mathrm{v}}_z-\hat{\mathrm{v}}_{z_0})^2}{\hat{t}}} \end{aligned} \tag{59}$$

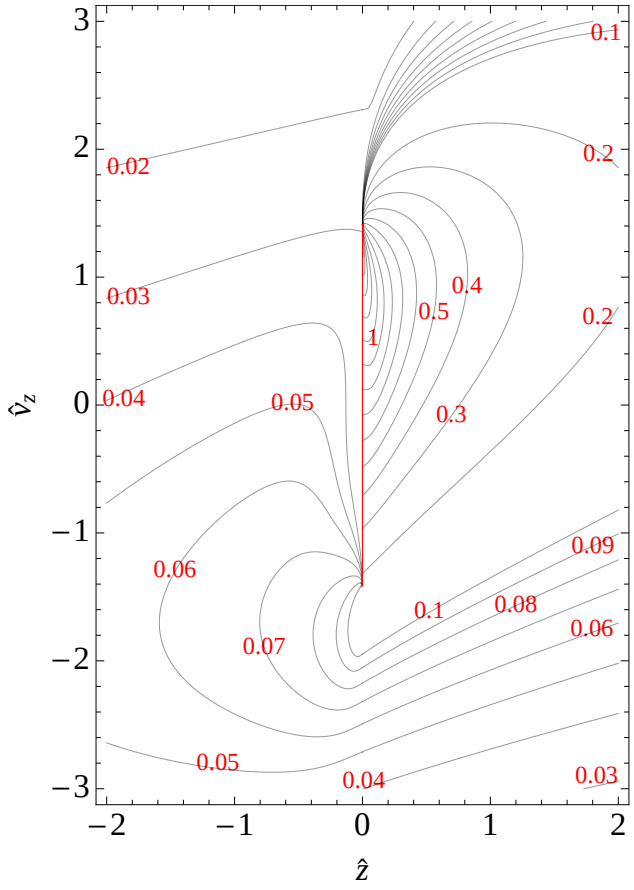

FIG. 11. Contour plot of the solution $f_{eq}(\hat{z}, \hat{\mathrm{v}}_z)$ to the equilibrium FP equation, Eq. (58). The red line at $\hat{z} = 0$ for $|\hat{\mathrm{v}}_z| < \sqrt{2}$ is the reflector.

via the integral

$$f_{\text{free}}(\hat{z}, \hat{\mathrm{v}}_z) = \int_0^{\sqrt{2}} d\hat{\mathrm{v}}_{z_0} \hat{\mathrm{v}}_{z_0}^2 \int_0^{\infty} d\hat{t}\, G(\hat{z}, \hat{\mathrm{v}}_z, \hat{t}; 0, \hat{\mathrm{v}}_{z_0})\,. \tag{60}$$

(Equation (59) is the solution of Eq. (43) in the absence of a reflector, i.e. for $A = 0$.) The large scale solution is displayed as a contour plot in Fig. 13.

The time integral in Eq. (60) must be carried out numerically in general, but in some special cases there are analytic expressions available. For example,

$$\int_0^{\infty} d\hat{t} G(0, \hat{\mathrm{v}}_z, \hat{t}; 0, \hat{\mathrm{v}}_{z_0}) = \frac{\sqrt{3}}{2\pi(\hat{\mathrm{v}}_z^2 + \hat{\mathrm{v}}_z \hat{\mathrm{v}}_{z_0} + \hat{\mathrm{v}}_{z_0}^2)}. \tag{61}$$

The result for $f_{free}(0, \hat{\mathrm{v}}_z)$ that follows from applying Eq. (61) to Eq. (60) is displayed in Fig. 12. As expected, at large velocities the free-particle distribution approaches the solution

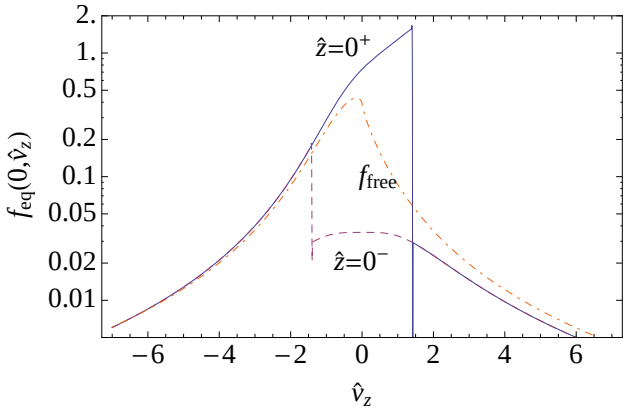

FIG. 12. Solution f_{eq} of Eq. (58) versus velocity for $\hat{z} = 0$ (shown using a log scale), on both the front and back faces of the reflector (i.e. $\hat{z} = 0^+$ and $\hat{z} = 0^-$). Note the discontinuities at $\hat{v}_z = \pm\sqrt{2}$. The slight oscillation in the solution at these discontinuities is an artifact of the grid. Also shown for comparison is the solution f_{free} in the absence of the reflector, given by Eq. (60).

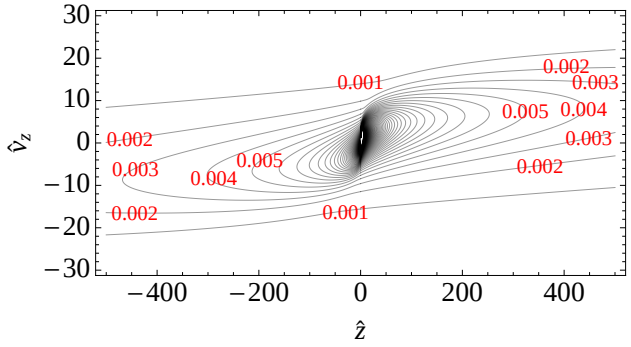

FIG. 13. Solution f_{eq} of Eq. (58) on large distance and velocity scales.

of Eq. (58).

The solution for $f_{\rm eq}$ is numerically integrated in Eq. (56) to obtain $\overline{h}_+ = 5.9008(2)$, where the estimated inaccuracy is due to the finite grid resolution. This value for $\overline{h}_+$ is in close agreement with the value found using Monte Carlo integration, $\overline{h}_+ = 5.899(1)$.

IX. DIFFUSION COEFFICIENT AND SLOWING-DOWN TIME

We now have enough information to evaluate the parallel velocity diffusion coefficient due to long-range (i.e. guiding-center) collisions given by Eq. (28). Noting that the maximum and minimum impact parameters are still λ_D and b respectively, and that long-range guiding

center collisions must have impact parameters larger than r_c, the limits on the remaining impact parameter integral in Eq. (28) are

$$D_i = \sum_j \left(\frac{e_i e_j}{m_i}\right)^2 n_j f_{ij}(0) \int_{\max(b,r_c)}^{\lambda_D} 2\pi \frac{d\rho}{\rho} \overline{h}([\rho/d]^{5/2}) \,. \tag{62}$$

Noting that $[\rho/d]^{5/2} = \overline{D}$, and using the results for $\overline{h}$ shown in Fig. 6, we see that the integral breaks into three pieces: one with $\rho \ll d$ where $\overline{h} = \overline{h}_+$ or $\overline{h} = \overline{h}_-$ (depending on the sign of the Coulomb interaction); another with $\rho \gg d$ where $\overline{h} = 2$; and the remaining piece, with ρ of order d. This third piece yields a constant of order unity whose value depends on the sign of the interaction, and which we call $C_\pm$. The sum of the three pieces gives D_i to logarithmic order, assuming that $\lambda_D/\max(b, r_c) \gg 1$:

$$D_i = \sum_j \left(\frac{e_i e_j}{m_i}\right)^2 n_j f_{ij}(0) 2\pi \{\bar{h}_\pm \; lnm(d/\max[b, r_c]) + 2 lnm(\lambda_D/\max[d, r_c]) + C_\pm\} \tag{63}$$

where $lnm(x) \equiv \ln(\max[1, x])$. The factor of 2 in front of the second logarithm is due to FP collisions with large impact parameters, while the factor of $\bar{h}_\pm$ in front of the first logarithm is due to 1D Boltzmann collisions with small impact parameters, enhanced by collisional caging in the case of repulsive interactions. This result has the form expected from Eq. (24), except that $\overline{h}_+ = 5.899$ rather than 4 because of collisional caging.

Note that $d/b \sim 1/\Gamma^{6/5}$ and $\lambda_D/d \sim 1/\Gamma^{3/10}$ where Γ is the Coulomb coupling parameter. Thus, in a weakly-coupled plasma with $\Gamma \ll 1$ the arguments of the logarithms in Eq. (63) are large, and depend on d, if the magnetic field is big enough so that $r_c < d$. One therefore typically neglects the constants $C_\pm$, because the logarithms are large. However, for completeness, the values of these constants are $C_+ = -3.1$ and $C_- = 1.3$. Note however that these values depend on the exact cutoffs used in obtaining the logarithms, and these values are beyond the scope of the theory presented here. For example, we don't know if the actual upper impact parameter cutoff is λ_D or $2\lambda_D$; we only know that it is of order λ_D. We therefore neglect the constants $C_\pm$ in what follows, noting that the logarithms are well-defined only up to constants of order unity.

Equation (63) includes only the 1D long-range collisions. To this one must add the effect of collisions that scatter the cyclotron velocity vector, arising from impact parameters in the

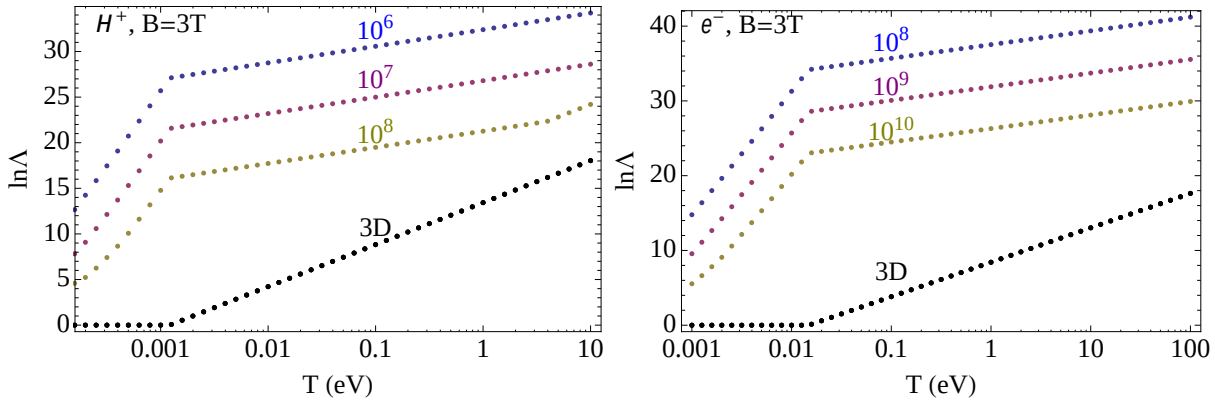

FIG. 14. Coulomb logarithm versus temperature for 3 densities (in cm^{-3}) and magnetic field $B = 3T$, for a) proton-proton collisions; b) $e - e$ collisions. Also shown is the 3D contribution, $(4/3)ln(r_c/b)$ (the lower dotted line).

range $\rho < r_c$. These 3D collisions are treated by the classical theory[6,7,16] and yield

$$D_i^{3D} = \sum_j \left(\frac{e_i e_j}{m_i}\right)^2 n_j f_{ij}(0) \frac{8\pi}{3} lnm(\min[r_c, \lambda_D]/b)\,. \tag{64}$$

The total diffusion coefficient is the sum of Eqs. (63) and (64), and the slowing rate is given by Eq. (2). The slowing down rate has the expected scaling, $\nu_i = \sum_j n_j \mathrm{v}_{ij} b^2 \ln\Lambda$ where $\mathrm{v}_{ij} = \sqrt{2\pi T\mu}/m_i$ and $\ln\Lambda$ is an improved "Coulomb logarithm" [given by the sum of the logarithms from Eqs. (63) and (64)]:

$$\ln\Lambda = \frac{4}{3} lnm(\min[r_c, \lambda_D]/b) + \overline{h}_{\pm} lnm(d/\max[b, r_c]) + 2lnm(\lambda_D/\max[d, r_c]). \tag{65}$$

This dimensionless factor is valid for any magnetic field strength, and is plotted versus temperature for proton-proton collisions in Fig. 14a and for electron-electron collisions in Fig. 14b. The factor is evaluated for three densities in the regime $r_c < \lambda_D$, and compared to the classical factor $4/3\ln(r_c/b)$ due to short-range 3D collisions. Note that in the weakly-magnetized regime where $r_c > \lambda_D$, only 3D collisions enter the logarithm; whereas in strongly-magnetized regime where $r_c < b$, only long-range collisions contribute to the slowing down since D_i^{3D} approaches zero[4] exponentially due to an adiabatic invariant associated with the collision dynamics.[17] More generally, long-range contributions to the Coulomb logarithm tend to dominate over 3D collisions at higher magnetic fields and at lower temperatures and densities.

X. SUMMARY

We have evaluated the collisional slowing rate for a weakly-coupled plasma in the regime $r_c < \lambda_D$, discovering several novel physical effects. The collisional slowing rate is enhanced by long-range guiding-center collisions. A new length scale d separates impact parameters into two ranges, one for $\rho > d$ where collisions are described by FP theory, and the other for $\rho < d$ where binary Boltzmann-like collisions occur. The slowing-down rate depends on the sign of the Coulomb interaction between colliding species. Finally, when the Coulomb interaction is repulsive, an enhancement of the slowing-down rate occurs, caused by "collisional caging".

Experiments are currently in progress that are operating in the regime $r_c < \lambda_D$, and that may be able to observe the enhanced collisional slowing effects discussed in this paper. One experiment measures the damping rate of magnetized plasma waves due to collisional drag between species in a multispecies nonneutral ion plasma.[18] A second experiment in a strongly-magnetized antimatter plasma uses collisional energy transfer from antiprotons to electrons to cool the antiprotons.[19]

The theory developed here assumes that the plasma is thermal, with a Maxwellian relative velocity distribution. It is fairly straightforward to generalize to non-Maxwellian distributions; this will be outlined in a future publication. For example, if the plasma has large-scale fluid motions, then shear in these motions can cause particle-particle interactions to be decorrelated faster than velocity diffusion predicts.[10] Such shears have been shown to limit test particle diffusion.[21]

If there is a shear rate s in the fluid velocity V (given by $s = |\nabla V|$), then particles are decorrelated in a time $1/s$ as they are pulled apart by the shear flow. The theory presented here is correct only if s is small enough so that $st_{\max} \ll 1$ where $t_{\max} \sim t_B/\overline{D}$ is the correlation time for 1D collisions without shear. This inequality depends on the collision impact parameter ρ, and the dependence can be estimated as $st_{\max} \sim (s/\nu)(b/\rho)$. Therefore $s < \nu$ is sufficient to ensure that the theory presented here is correct for all impact parameters that enter Eq. (63). The effect of larger shears on the slowing rate will be considered in future work.

Previous transport theories of 1D long-range interactions[10,12,13,15] have not considered the effect of small-impact-parameter Boltzmann collisions. The previous work, based on FP theory, needs to be re-evaluated to account for such collisions. For the coefficients of

viscosity and thermal conduction, which are dominated by collisions with impact parameters of order λ_D or larger, we believe that Boltzmann collisions will have a negligible contribution. The same cannot necessarily be said for the coefficient of cross-magnetic field test particle diffusion,[10] where impact parameters less than d can contribute. We will consider the effect of Boltzmann collisions on cross-magnetic field test particle diffusion in future work.

The author thanks Profs. C. F. Driscoll and T. M. O'Neil for useful discussions. This work was supported by NSF grant PHY0903877 and DOE grant DE-SC0002451.

APPENDIX A: NUMERICAL SOLUTION OF THE FP EQUATION

In order to solve Eq. (58) for $f_{eq}(\hat{z}, \hat{\mathrm{v}}_z)$ numerically, we use a nonuniform grid, transforming $\hat{z}$ and $\hat{\mathrm{v}}_z$ to new variables s_z and s_v through the transformation $\hat{z} = \hat{z}(s_z)$ and $\hat{\mathrm{v}}_z = \hat{\mathrm{v}}_z(s_\mathrm{v})$. We choose

$$\begin{aligned} \hat{z} &= s_z/(1-s_z^2)^3\,, \qquad -1 < s_z < 1 \\ \hat{\mathrm{v}}_z &= s_\mathrm{v}/(1-s_\mathrm{v}^2)^3\,, \qquad -1 < s_\mathrm{v} < 1 \end{aligned} \tag{A1}$$

so that the grid is densest for $\hat{z}$ and $\hat{\mathrm{v}}_z$ of 0(1), but extends to infinity. In these coordinates Eq. (58) becomes

$$\hat{\mathrm{v}}_z(s_\mathrm{v})u_0(s_z)\frac{\partial f_{eq}}{\partial s_z} = u_1(s_\mathrm{v})\frac{\partial f_{eq}}{\partial s_\mathrm{v}} + u_2(s_\mathrm{v})\frac{\partial^2 f_{eq}}{\partial s_\mathrm{v}^2} \tag{A2}$$

where $u_0(s_z) = 1/\partial\hat{z}/\partial s_z$, $u_1(s_\mathrm{v}) = u_0(s_\mathrm{v})\partial u_0/\partial s_\mathrm{v}$, and $u_2(s_\mathrm{v}) = u_0^2(s_\mathrm{v})$. The source term in Eq. (58) is accounted for in the boundary conditions, as described below.

We then use a uniform grid in (s_z, s_v) choosing

$$s_z = m\Delta z\,, \qquad m = -M_z+1,\, -M_z+2, \ldots,\, M_z-2,\, M_z-1 \tag{A3}$$

and

$$s_\mathrm{v} = (n+1/2)\Delta\mathrm{v}\,, \qquad n = -M_\mathrm{v}, \ldots,\, M_\mathrm{v}-1 \tag{A4}$$

where $\Delta z = 1/M_z$ and $\Delta\mathrm{v} = 1/(M_\mathrm{v}+1/2)$.

Boundary conditions are $f_{mn} = 0$ for $m = \pm M_z$ or $n = M_\mathrm{v}$ or $n = -M_\mathrm{v}-1$ (i.e. $f_{eq} = 0$ at infinity). In order to deal with the reflector and the source at $z = 0$ we break f_{mn} into a solution f^+_{mn} for $z \geq 0^+$, and a solution f^-_{mn} for $z \leq 0^-$. The $z = 0$ boundary conditions are then

$$\begin{aligned} f^-_{0n} &= f^-_{0,-n-1}\,, & -\sqrt{2} \leq \mathrm{v}_n \leq 0 \\ f^-_{0n} &= f^+_{0,n}\,, & |\mathrm{v}_n| > \sqrt{2} \\ f^+_{0n} &= f^+_{0,-n-1} + \mathrm{v}_n\,, & 0 \leq \mathrm{v}_n \leq \sqrt{2} \end{aligned}$$

where $\mathrm{v}_n = \hat{\mathrm{v}}_z(s_\mathrm{v}(n))$ is the velocity at grid point n. The first boundary condition is the reflecting condition on the rear face of the reflector, the second is the continuity condition beyond the reflector, and the third is the reflecting condition on the front face, including the effect of the source term in the equation. Thus, f^+_{0n} is the value of f for z just greater than the source at $z = 0^+$.

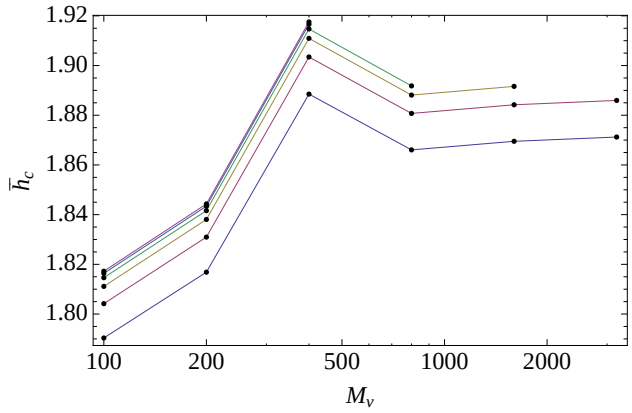

FIG. 15. Values of $\overline{h}_c$ obtained versus grid resolution. Connected dots from smallest to largest $\overline{h}_c$ values have $M_z = 100$, 200, 400, 800, 1600 and 3200 repectively.

The equations for f^+ and f^- are finite-differenced on the grid using the Crank-Nicholson method.[22] The method is second-order accurate in both $\Delta \mathrm{v}$ and Δz.

The finite-differenced equations are then

$$\mathrm{v}_n u_{0n} \frac{f^{\pm}_{mn} - f^{\pm}_{m-1\,n}}{\Delta z} = \frac{1}{2} u_{1n} \left(\frac{f^{\pm}_{mn+1} - f^{\pm}_{mn-1}}{2\Delta \mathrm{v}} + \frac{f^{\pm}_{m-1\,n+1} - f^{\pm}_{m-1\,n-1}}{2\Delta \mathrm{v}} \right) + \frac{1}{2} u_{2n} \left(\frac{f^{\pm}_{mn+1} - 2f^{\pm}_{mn} + f^{\pm}_{mn-1}}{\Delta \mathrm{v}^2} + \frac{f^{\pm}_{m-1\,n+1} - 2f^{\pm}_{m-1\,n} + f^{\pm}_{m-1\,n-1}}{\Delta \mathrm{v}^2} \right). \tag{A5}$$

In Fig. 15 we show values of $\overline{h}_c$ obtained by numerical integration of Eq. (56) for different values of M_v and M_z up to $M_\mathrm{v} = 3200$ and $M_z = 3200$. By extrapolation of the results we obtain $\overline{h}_c = 1.9008$. The extrapolation uses the fact that for fixed M_v the difference in $\overline{h}_c$ values for different values of M_z is almost independent of the value of M_v chosen. We may therefore extrapolate the $M_\mathrm{v} = 200$ dataset to infinity and add this value to the value $\overline{h}_c\,(M_\mathrm{v} = 3200,\, M_x = 200) - \overline{h}_c(M_\mathrm{v} = 200,\, M_x = 200)$. Repeating this for $M_\mathrm{v} = 400$, 800 or 1600, we obtain nearly identical values of $\overline{h}_c$. The values obtained are $\overline{h}_c = \{1.9002,\, 1.9012,\, 1.9007,\, 1.9009\}$ for $M_\mathrm{v} = \{200,\, 400,\, 800,\, 1600\}$ respectively, and the mean of these values is the stated result, $\overline{h}_c = 1.9008$. The RMS error in these values, 2×10^{-4}, is fairly small. However, the actual error in the result could be bigger if our extrapolation method is incorrect. It would be better to simply increase M_z and M_v by, say, a factor of 10, but we cannot do so at this time due to limitations in available computer memory.

REFERENCES

[1]F. F. Chen, *Introduction to Plasma Physics and Controlled Fusion, Vol. 1* (New York: Springer, 2006), p. 182.

[2]H. Goedbloed and P. Stefann, *Principles of Magnetohydrodynamics* (Cambridge, UK: Cambridge Univ. Press, 2004), p. 163. f

[3]P. Bellan, *Fundamentals of Plasma Physics* (Cambridge, UK: Cambridge Univ. Press, 2006), p. 292.

[4]T. M. O'Neil, Phys. Fluids **26**, 2128 (1983).

[5]L. Spitzer, *Physics of Fully Ionized Gases* (New York: Interscience, 1956), p. 76.

[6]S. Ichimaru, *Basic Principles of Plasma Physics* (London: W.A. Benjamin Inc., 1973), p. 242.

[7]A. Simon, Phys. Rev. **100**, 1557 (1955).

[8]C. L. Longmire and M. N. Rosenbluth, Phys. Rev. **103**, 507 (1956).

[9]M. N. Rosenbluth and A. N. Kaufmann, Phys. Rev. **109**, 1 (1958).

[10]D. H. .E. Dubin, Phys. Rev. Lett. **79**, 2678 (1997).

[11]F. Anderegg, X.-P. Huang, C. F. Driscoll, E. M. Hollmann, T. M. ONeil, and D. H. E. Dubin, Phys. Rev. Lett. **78**, 2128 (1997).

[12]T. M. O'Neil, Phys. Rev. Lett. **55**, 943 (1985).

[13]D. H. E. Dubin and T. M. ONeil, Phys. Rev. Lett. **78**, 3868 (1997).

[14]E. M. Hollmann, F. Anderegg and C. F. Driscoll, Phys. Rev. Lett. **82**, 4839 (1999).

[15]D. H. E Dubin, "Plasma Collisional Transport," in *Les Houches Lectures on Long Range Interacting Systems*, T. Dauxois, *et al.*, eds. (Oxford: Oxford Univ. Press, 2010).

[16]N. Rostoker, Phys. Fluids **3**, 922 (1960).

[17]M. Glinsky and T. M. O'Neil, Phys. Fluids **B**3, 1279 (1991).

[18]M. Affolter, F. Anderegg, C. F. Driscoll, M. Anderson and T. M. O'Neil, "Damping of Plasma Modes in Ion Plasmas," Bull. Am. Phys. Soc. **56**, 76 (2011).

[19]B.G. Andresen *et al.* (ALPHA Collaboration), Phys. Rev. Lett. **106**, 145001 (2011).

[20]C. Gardiner, *Stochastic Methods* (Springer, NY, 2009).

[21]D. H. E. Dubin and D.-Z. Jin, Phys. Lett A **284**, 112 (2001); C. F. Driscoll, F. Anderegg, D. H. E. Dubin, D.-Z. Jin, J. M. Kriesel, E. M. Hollmann, and T. M. O'Neil, Phys. Plasmas **9**, 1905 (2002).

[22]W. H. Press, B. P. Flannery, S. A. Teukolsky and W. T. Vetterling, *Numerical Recipes* (Cambridge University Press, London, 1986).